The Advanced Implantation Detector Array (AIDA)

O. Hall, T. Davinson, C. Griffin, C. Appleton, C. G. Bruno, A. Estrade, D. Kahl, L. Sexton, P. J. Woods

School of Physics and Astronomy, University of Edinburgh, Edinburgh, EH9 3FD, UK

I. Burrows, P. J. Coleman-Smith, M. Cordwell, A. Grant, M. Kogimtzis, M. Labiche, J. Lawson, I. Lazarus, V. F. E. Pucknell, J. Simpson, C. Unsworth

STFC Daresbury Laboratory, Daresbury, Warrington, WA4 4AD, UK

D. Braga, M. Prydderch, S. L. Thomas

STFC Rutherford Appleton Laboratory, Didcot, OX11 0QX, UK

L. J. Harkness-Brennan, P. J. Nolan, D. Seddon, R. D. Page

Department of Physics, University of Liverpool, Liverpool, L69 7ZE, UK

Abstract

The Advanced Implantation Detector Array AIDA is a state-of-the-art detector system for the measurement of the decay properties of exotic nuclei at leading fragmentation/fission facilities. Built around highly segmented double-sided silicon strip detectors the positions of both implanted ions and their subsequent decays are measured with high precision which allows for efficient ion-β correlations, even at high implantation rates. A summary of the system and the analysis methodologies used are presented.

Keywords: Fragmentation, DSSD, Implantation

1. Introduction

Decay spectroscopy experiments are a useful tool for probing the properties and structure of radioactive nuclei. The information obtained is relevant to both theories of nuclear structure and also to nuclear astrophysics. In nuclear astrophysics today, many of the questions revolve around the r-process [1] - the astrophysical process responsible for the production of around half the elements heavier than iron. The nuclei of importance to the r-process and, therefore, the most desirable to study are very far from stability and often have short decay lifetimes of less than a second. Obtaining experimental information on these nuclei requires them to be observed soon after they are produced.

In-flight fragmentation or fission of heavier nuclei, such as ^{238}U and ^{124}Xe, are common production methods employed that are well suited to the study of short-lived exotic nuclei. Exotic nuclei are produced as the heavy nuclei, accelerated to high-energies of 100s of MeV/u, are impinged on a thin target causing them to undergo fragmentation or fission reactions producing a wide range of exotic nuclei. Fragment spectrometers are then used to filter, focus and identify the produced ions, delivering a cocktail beam of many isotopes surrounding a central isotope of interest to a detector located at the end of fragment spectrometer within just a few hundreds of ns of the creation of the ion [2]. The detector is then able to measure the subsequent decay of the implanted nuclei. An additional benefit of these methods is the delivery of multiple different species to the experimental area, which can be studied simultaneously. However, random correlations can be a problem in such measurements. Random correlations occur when you ascribe the decay of an implanted ion to the incorrect implanted ion, which results in the formation of background in a measurement. The risk of random correlations being made increases with implantation rate and can be particularly challenging when the mean time between implants is greater than the mean lifetime of the nuclei being implanted.

One method to reduce the number of random correlations made is to use positional information in addition to temporal information when correlating implanted ions with subsequent decays, requiring decays to be observed in the same region of the detector as implanted ions. This technique has been in use since the early 1980s, for example one-dimensional position sensitive detectors were used to correlate the positions of direct proton emission events with implanted ions of ^{151}Lu [3]. By the late 1980s this technique had been further expanded to use a two-

Email address: oscar.hall@ed.ac.uk (O. Hall)

dimensional position sensitive silicon surface barrier detector allowing the area over which correlations are made to be further restricted [4, 5]. Increased sensitivity with the technique was achieved with the move to double-sided silicon strip detectors (DSSDs), improving on both the positional and energy resolution over the previous silicon surface barrier detector [6]. These first DSSDs were optimised for the study of proton and alpha decays from radioactive species produced in fusion evaporation reactions. Their thicknesses ranging from $67 - 110$ μm were optimised to sufficiently stop fusion evaporation products, alpha particles and protons, while being effectively transparent to β-particles reducing the β-background that would otherwise be observed by the detectors.

Modern fragmentation facilities require detectors to be much thicker than these early detectors as the stopping distribution of different isotopes can cover a range of a few mm in Si. Fortunately, advances in the manufacturing process of DSSDs since these early models have permitted the production of detectors with both larger active areas and increased thicknesses. Larger active areas allow for greater positional separation of the implanted ions, further reducing the number of random correlations, while greater thicknesses make the detectors more suited to the stopping of high-energy recoil ions produced at current fragmentation facilities. Examples of systems utilising positional correlations at fragmentation facilities include a β-counting system for fast fragmentation beams at NSCL [7], the Silicon IMplantation Beta Absorber (SIMBA) used at GSI [8] and RIKEN's WAS3ABi (wide-range active silicon-strip stopper array for beta and ion detection) [9]. A challenge common to these systems is the wide range of energies across implantation and decay events which take place. Stopping ions can deposit more than 10 GeV in a detector while β-particles can deposit less than 1 MeV.

The Advanced Implantation Detector Array (AIDA) represents the next generation of state-of-the-art silicon detector arrays for performing implant-decay correlation measurements. The system was originally developed for use at FAIR, with one of the principal motivations being the study of β-decay properties of relevance to the astrophysical r-process[10]. Coupling large area, high segmentation silicon detectors with state-of-the-art fast electronics, AIDA can positively correlate implanted ions and subsequent decays at high implantation rates. At present two AIDA systems are currently in use. The first is currently located at the Radioactive Ion Beam Factory [11] at RIKEN, Japan and has been in use since 2016. The second is located at GSI and has been used as part of FAIR Phase 0 since 2020 within the DESPEC collaboration [12]. At both facilities AIDA is used alongside other detector arrays such as BRIKEN [13], DTAS [14], FATIMA [15] or DEGAS [16, 17] providing additional, complimentary information of decay modes involving gamma-rays and neutrons.

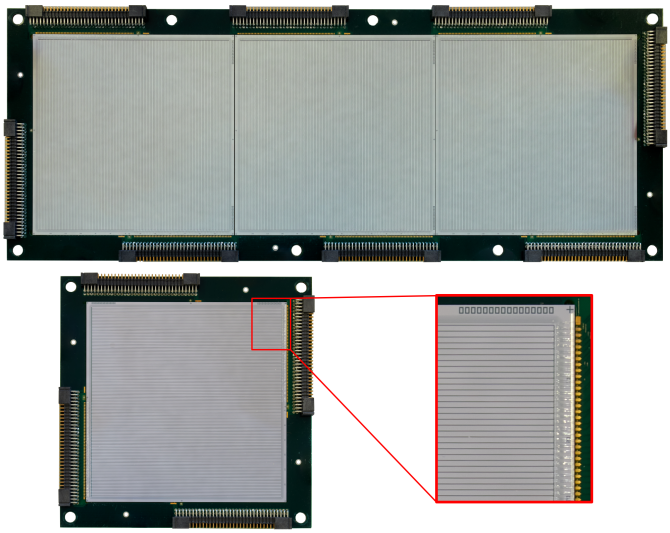

Figure 1: Top image: Photograph of the 'triple' DSSD consisting of three 8×8 cm^2 wafers bonded together. Lower left image: Photograph of the 'single' DSSD consisting of a single 8×8 cm^2 wafer. Lower right image: Zoomed in section of the single wafer, highlighting the individual strips and their bond wires.

2. AIDA hardware

2.1. Double-sided Silicon Strip Detectors

As mentioned in the introduction the use of position sensitive detectors is hugely beneficial in the reduction of random correlations when performing implant decay measurements. Position sensitive detectors are available in many forms each with their own sets of benefits and drawbacks. In the case of AIDA the decision was made to go with segmented silicon detectors, enabling a high degree of positional resolution while still providing the energy resolution required for spectroscopic quality measurements. It is a stack of these highly segmented Double-sided Silicon Strip Detectors (DSSDs) that characterise AIDA. The AIDA system makes use of two differently sized DSSDs depending on the physics aims of the experiment. Common to both sizes of DSSD is the nominal thickness of 1000 μm, strip pitch of 560 μm, and inter-strip separation of 50 μm. The thickness of 1000 μm is ideal for use at fragmentation facilities where the energy spread of ions results in a stopping distribution that spans up to a few mm in Si. Here with a stack of just a few detectors many ions can be effectively stopped with a single degrader setting while still allowing different atomic species to be spread throughout the stack adding an additional degree of position separation. A thickness of 1 mm also increases the detection efficiency of β-electrons when compared to earlier thin detectors thanks to the increased energy deposition before escaping the detector. The narrow strip pitch of 560 μm provides a high degree of segmentation, allowing the positions of events to be determined with high accuracy across the surface of the detector.

The smaller of the two DSSD sizes available consists a single Si wafer with an active area of 7.63 cm $\times$ 7.63 cm,

segmented into 128 strips on each side arranged orthogonally resulting in 16,384 voxels per DSSD. A photograph of this DSSD is shown in the lower panel of Figure 1. The relatively small transverse dimensions make the detector well suited to being paired with additional detector systems that require high volumetric efficiency around the point of implantation. Examples of these systems include DTAS [14] and BELEN/BRIKEN [18, 13], all of which benefit from being able to maximise the volume surrounding the DSSDs that is covered by a detector in order to maximise their detection efficiencies.

The second size of detector has been designed to exploit the spatial separation of isotopes in the x direction achievable with the future Super-FRS project [19] at FAIR [20] and with the current FRagment Seperator (FRS) [21] at GSI during FAIR Phase-0. With an active area of $\approx$ 24 cm $\times$ 8 cm and segmented into 384 $\times$ 128 strips, different isotopic species are implanted into distinct regions across the detector minimising random correlations between species. A detector of this size is larger than what can be reasonably achieved from a single Si wafer, the detectors are instead formed by bonding together the n^+n strips of three of the 8×8 cm^2 wafers to form one large detector. The benefit of this approach over the use of three smaller detectors is the reduction in electronics channels required to readout signals. For the bonded triple detector a total of 1024 channels are required compared to the 1536 that would be required to run three individual smaller detectors. A secondary benefit is the minimised loss in dead area between active areas, when comparing the gap between wafers on the wide detector (Upper panel of Figure 1) it can be seen that the distance between individual wafers is much smaller than if three overlapping detectors were used. As different isotopes are now spread across the surface of the detector there is less need to spread them across multiple detectors in the stack. The use of wedge shaped degraders then allows a single detector to be used to stop all the isotopes of interest providing a greater stopping power for lighter elements than heavier elements.

2.2. Mechanical assembly

As mentioned in the introduction, one of the primary uses of active stoppers is in decay spectroscopy measurements where one of the decay products is a charged particle. Examples of this can be direct proton emission and β-decay studies. Often these decays leave the daughter nucleus in an excited state and it is desirable to observe the de-excitation of the nucleus whether that be through γ-ray emission or particle emission. For the cases where the de-excitation does not proceed through charged particle emission and instead proceeds through a mode which the DSSDs are not sensitive to it is desirable to have other detector types sensitive to the emission mode as close to the site of the decay as possible to maximise the detection efficiency. AIDA achieves this by mounting the detectors at the end of thin stainless steel rods within a thin, light-tight Al enclosure which is known as the "snout". The

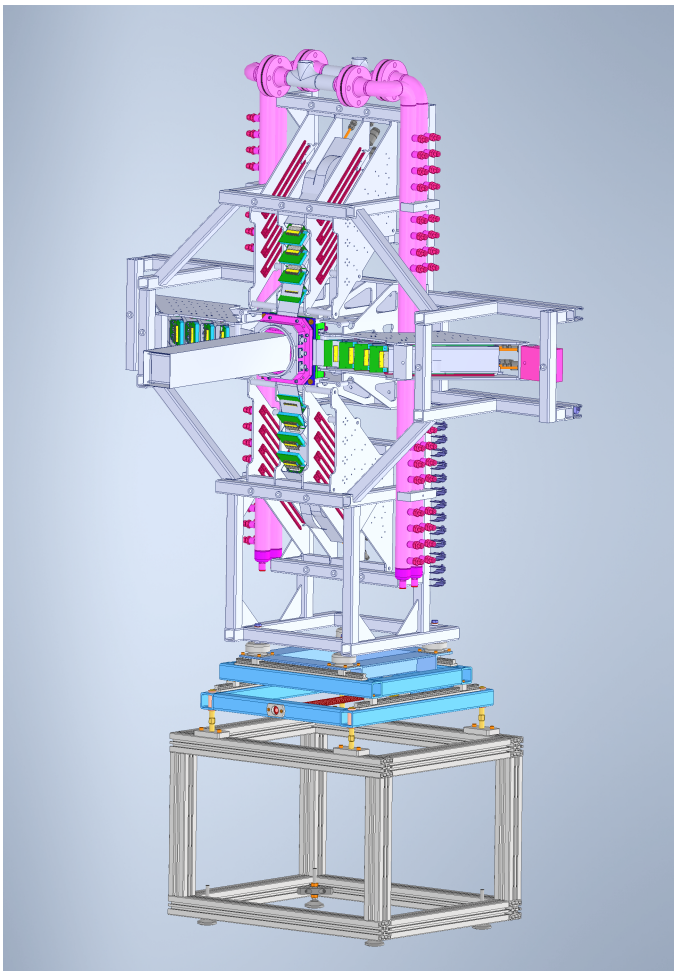

Figure 2: CAD model of the AIDA version currently installed at GSI. The "snout" shown is of dimensions to house the narrow 8×8 cm^2 DSSDs. Green boards arranged at 0°, 90°, 180° and 270° around the "snout" are the adaptor boards that connect the DSSD cabling (not shown) to the FEEs. Pink pipes are water cooling manifolds which distribute cooling water to each of the FEEs. The structure is designed to be easily expanded in the horizontal direction to support the 24 cm $\times$ 8 cm DSSD.

cables for the detectors run alongside the inner surface of the "snout" enclosure, keeping the central region free for the passage of ions. The cables then exit the enclosure at the base of the "snout" where they are connected to the readout electronics. The length of the "snout" enclosure is chosen such that the DSSD and thus the decay site can be located at the centre of the additional detector systems, typical distances from the DSSD to readout electronics are in the range of $\sim 60 - 100$ cm. To minimise the scattering and attenuation of radiation the material budget surrounding the detectors is kept to a minimum, an example of this is that Al snout enclosure is just 0.5 mm thick. The DSSD operate in air.

2.3. Read out electronics

To minimise the amount of noise introduced to the signal between the DSSD and the electronics it is desirable to

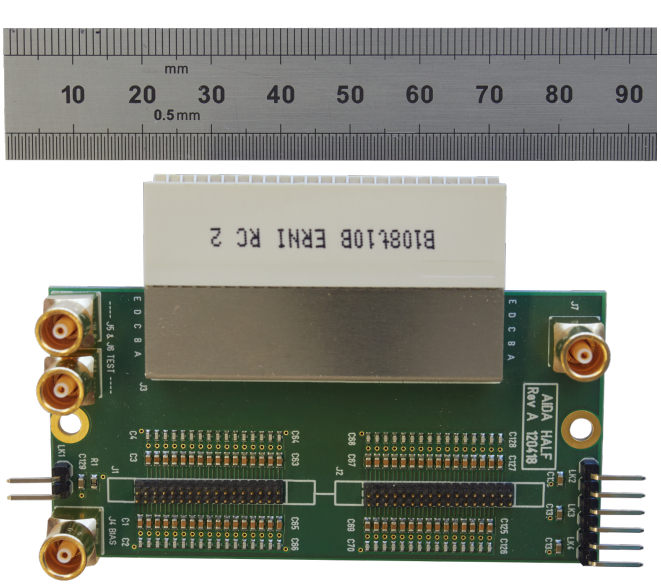

Figure 3: An example adaptor board used for connecting the FEE module to the detector cabling. LEMO connections provide connections for a test input (top left), bias line (bottom left) and the ground plane (top right). Jumper pins allow optional grounding of various parts of the detector package. High-density IDC connectors (middle) are connected to the DSSD cabling.

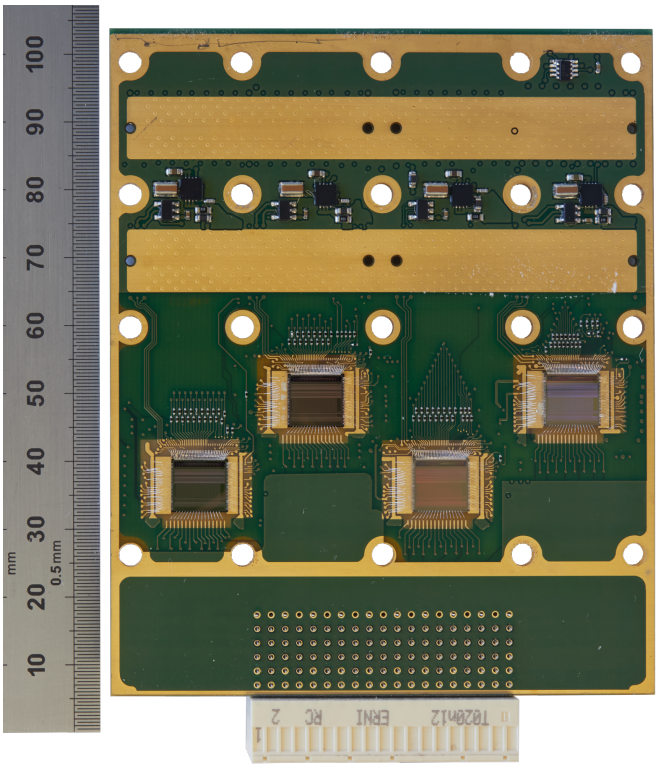

Figure 4: Photograph of the FEE mezzanine board. The four ASIC chips that are wire bonded to the board are visible in the lower half. 95-pin ERNI connector [24] shown at the bottom. Connectors to the FEE64 PCB not shown (reverse side of ASIC PCB).

have the electronics located as close the DSSD as possible. With detector stacks that require over 1000 channels of instrumentation, providing instrumentation for all of these channels close to the DSSD is a challenge requiring the use of high-density electronics. In the following sections the components in the chain from DSSD to data-acquisition are detailed.

2.3.1. Detector cabling and adaptor boards

Electrical connections to the DSSD are made over low profile 68 pin Samtec FTSH headers [22]. Each connector provides readout for 64 strips on the DSSD and provides additional connections for PCB ground, detector bias and field plates. Short ($\sim$ 105 mm) kapton couplers provide a low profile, minimal material, intermediate connection from the DSSD to bulkier Samtec ribbon cables [23] further along the snout where there is less requirement to minimise the material budget. The use of screened kapton cables for the full length between DSSD and electronics was found to result in large capacitative load for the preamplifers and unacceptable noise performance.

The ribbon cables exit at the base of the snout and connect to PCB (printed circuit board) adaptor cards, illustrated in Figure 3, which act as the interface between the detector cabling and the readout electronics. Traces on the PCB map the signals from the DSSD to an ERNI input connector [24] to the front end electronics. LEMO connectors on the PCB provide detector bias and test inputs. Typical values for the test and ac coupling capacitors on the board are 0.7 pF (same as LEC C_f providing unity gain test input) and 33 nF/100 V/X7R respectively. The upper right connector (Figure 3) is a high-quality connection to the PCB ground. Jumper pins seen on the left and right of the adaptor board in Figure 3 allow parts of the DSSD such as the DSSD PCB, and the front and back field plates to be grounded to the adaptor card PCB ground which in turn can be connected to a mechanical ground via the LEMO connector.

The use of a simple adaptor PCB between the DSSD and front end electronics means that it is straightforward to use other silicon strip detector designs as required. For example, AIDA hardware has been used with MSL type W1 (16×16, 50×50 mm^2), BB7(32×32, 64×64 mm^2) and TTT14 (128×128, 98×98 mm^2) [25] detectors.

2.3.2. Application Specific Integrated Circuits (ASICs)

One of the design goals of the AIDA electronics was to provide good energy resolution for both the implanted ions and also their subsequent decays. In the case of β-decay experiments β-particles will deposit energies ranging from 10s of keV up to a few MeV in the DSSD whereas stopping implanted ions can deposit up to 17 GeV. This defines an energy scale where the minimum energy we hope to measure in our system is one-millionth of the maximum possible energy deposition. To provide good energy resolution across this broad range of energies poses a significant challenge in the handling of signals. To meet these re-

quirements, a 16-channel Application Specific Integrated Circuit (ASIC) was designed to handle the readout of the signals. A detailed description of the design of the ASIC can be found in Ref. [26], however, a short description of the features that provide the required functionality is presented here.

One of the defining features of the AIDA ASIC is found in it's analogue front end, where each strip is connected to two preamplifier - and subsequent signal processing - channels. The first is the high energy channel (HEC) with a low gain preamplifier for measuring high energy implants. The second channel is connected to a preamplifier with selectable gain - a low energy channel (LEC) with high gain for measuring low energy radioactive decays, and a medium energy channel (MEC) with intermediate gain for measuring higher energy ions. AIDA is therefore able to provide high resolution measurements across a wide range of energies. The selectable gain channel allows the Full Scale Range (FSR) to be set to either 20 MeV or 1 GeV, whereas the low-gain preamplifier has a FSR of $\approx$ 20 GeV (Maximum energy deposition of ^{238}U in 1 mm Si $\approx$ 16.6 GeV).

The preamplifiers are configured such that only the selectable-gain preamplifier is directly connected to the input channel, while the low-gain preamplifier is connected via a bypass link. When a small energy signal is input, such as a decay event, only the selectable-gain amplifier is connected to the input and the signal processing is handled entirely within this circuit. However, when a high-energy implant event occurs the charge deposited in the detector saturates the selectable-gain channel and a CMOS bypass switch opens, providing a path to the low-gain preamplifier. This connection is maintained until the integration of the input charge is complete. Once the integration of the input charge is complete and the peak is held in a peak hold circuit the low-gain preamplifier is disconnected from the input. A series of pulses are then sent to the high-gain/low-energy channel to remove the charge and return the signal to baseline. This allows the circuit to be ready to measure new signals in as little as a few tens of microseconds following the large implant signal, removing the need to wait many time constants of an *RC* circuit in conventional electronics.

The availability of the dedicated low-gain/high-energy channels is one of the features that sets AIDA apart from previous iterations of active stoppers. Often in these previous generation of detectors, logarithmic preamplifiers were used to handle the high-energy signals, effectively losing any energy information about the incoming implant. With AIDA this energy information is not lost and we have demonstrated an energy resolution of $\sim$ 20 MeV or $\sim$ 0.1% FSR. The typical dynamic range of an ASIC is $\sim 1:2000$. The additional information provided by the energy of the stopping ions can be used as an additional measure of the Z of the implanted nuclei and also the discrimination of charge states, a common contaminant in the particle identification spectra produced by fragment separators.

A summary of the performance and specifications of the AIDA ASIC can be found in table 1.

No. channels	16
Input polarity	positive & negative
Gain	HEC **and** LEC **or** MEC
Low energy channel (LEC)	20 MeV FSR
Medium energy channel (MEC)	1 GeV FSR
High energy channel (HEC)	20 GeV FSR
Noise e_0 ($\tau = 8\mu$s)	
LEC	$<$ 10 keV rms
MEC	$<$ 500 keV rms
HEC	$<$ 20 MeV rms
Noise slope e_{ns} (LEC, $\tau = 8\mu$s)	**TBC** eV/pF rms
Integral non-linearity	0.1% $>$ 90% FSR
Shaping time (4 bit register)	$0.5 - 8$ μs, 0.5 μs increment
Slow comparator (8 bit register)	
LEC	10 keV/LSB
MEC	500 keV/LSB
Fast comparator (8 bit register)	
LEC	100 keV/LSB
MEC	5 MeV/LSB
HEC	100 MeV/LSB
Multiplex readout	32 : 1
ASIC Clock	500 kHz
Power	**TBC**
Die Size	7.9×7.5 mm^2
Process	AMS 0.35 μm CMOS

Table 1: AIDA ASIC specifications

2.3.3. Front End Electronics

The electronics that handle the data output of the AIDA ASIC are mounted on a module that is known as the Front End Electronics (FEE64) module. Each FEE64 module is responsible for handling the signals from 64 channels of instrumentation, the number of strips handled by one connector on the DSSD. The FEE64 modules contain all of the electronics used in the processing of the signals and act as their own independent data acquisition systems. The requirements for these modules was that they need to be both relatively compact, to allow them to be located close to the DSSD, and also that they need to be able to handle a high throughput of data, to support the high beam intensities available at modern fragmentation facilities.

At the front of the FEE module are four ASICs wire bonded onto a mezzanine board which provides the signal processing for the 64 channels of instrumentation the FEE is responsible for. In operation these mezzanine boards are covered with a copper plate which acts as an EMI/RFI shield and also a cooling plate to dissipate excess heat while providing a light tight enclosure for the ASICs. Figure 4 shows one of these mezzanine boards without the copper plate, the four ASIC chips are arranged on the lower half of the board. Each ASIC is connected via a 32:1

multiplexer to an Analog Devices 7980 16-bit, 1 MSPS ADC [27] with an input range of ±2 V. ASIC channels with valid data are sequentially readout via the multiplexer controlled by a 500 kHz clock. As the FEEs process signals of both polarities zero output nominally corresponds to ADC channel 32768 with FSR positive and negative signals corresponding to ADC channels 0 and 65536 respectively. This works out to be about 0.7 keV/ch for the LEC and 0.7 MeV/ch for the HEC.

The ADC readout, data processing, building of events, and control of the FEE64 is handled by a Xilinx Virtex 5 [28] Field Programmable Gate Array (FPGA) which includes an embedded PowerPC processor. The data acquisition program runs on the Linux operating system installed on the PowerPC processor. Each FEE64 is therefore a fully integrated and independent data acquisition system. ADC data is stored using the Total Data Readout (TDR) GREAT data format [29], with each data item stored as a pair of 32bit words. Contained in these words is the ADC value itself, a partial timestamp relative to the FEEs internal 100 MHz clock, a flag indicating whether it was from the high or low gain amplifier, and information on the channel and FEE in which the event was recorded. In addition to the ADC data items, information data items are included in the data stream which provide information on the running of the FEE and also contain the required information to reconstruct the full timestamp of ADC events.

The AIDA ASIC preamplifier outputs are also conencted (via signal conditioning op-amps) to eight Analog Devices 9252 Octal, 14-bit, 50 MSPS ADCs [30]. With these, the waveforms of signals in each of the low-energy preamplifiers can be observed, a useful tool in debugging and investigating the noise performance of the electronics. There is also the ability to record or process the waveforms of events to file. While this feature has not yet been utilised in operation it would allow additional offline analysis to be performed on the waveforms such as pulse shape discrimination.

Synchronisation is maintained between each of the FEE cards via the use of an external 50 MHz clock, which is provided to each of the FEE cards over a High Definition Multimedia Interface (HDMI) connection. To date two different timestamping and synchronisation systems have been used. For experiments at RIKEN using AIDA as part of BRIKEN, the timestamp was a 48 bit scaler which incremented in 10 ns intervals and synchronisation was maintained between systems with a correlation scaler as detailed in Ref [18]. In experiments at GSI the timestamp was stored as a 64-bit number representing the time in ns. Here the timestamp was externally provided by the WhiteRabbit system [31] which provides a common timestamp to the entire facility allowing all systems to be aligned in time to high precision. As both of these timestamp values would take up too much of the available 64-bits of space in the GREAT data format event words the timestamp is split into multiple parts. The lowest 28 bits of the timestamp is attached to every event whereas the upper bits of the timestamp are instead added to the datastream at fixed intervals as SYNC statements with a rate greater than the rollover period of the bits.

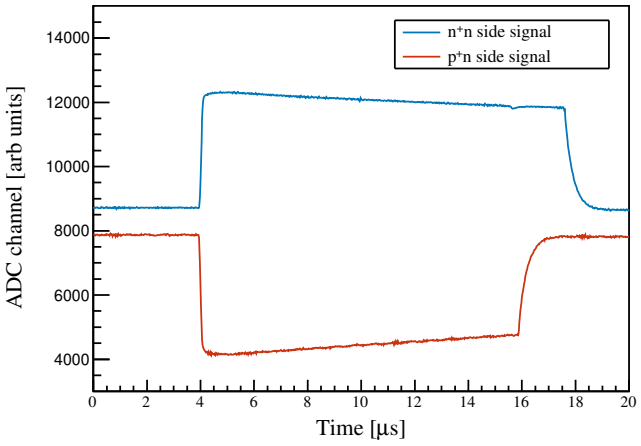

Figure 5: Example waveform output from the 50×10^6 samples per second ADC located on the FEE card. Signals were triggered by a common positive polarity pulser with polarity for n^+n strips inverted with a Cooknell SA1 Sum & Invert Amplifier.

3. AIDA in operation

3.1. DAQ Control

With each single DSSD requiring 4 FEE cards and each triple DSSD requiring 8 FEE cards it is not unimaginable that an experiment could require upwards of 24 FEE cards in total. Controlling each of the FEEs individually would not be feasible, instead, commands are issued from a central server which then communicates with each of the embedded CPUs on the FEE cards. From the server the user is able to reset, setup, start and stop the data acquisition program running on each embedded processor. The user can also configure, control and monitor all aspects of ASIC and FEE64 operations, for example, specifying the ASIC input signal polarity, shaping time, and comparator thresholds.

The data acquisition program running on the FEE64 embedded processor creates a number of spectra which are stored in memory on the FEE card. The spectra show LEC (or MEC) and HEC ADC data, ADC and fast comparator hit patterns, and preamplifier waveforms. An example of preamplifier output signal waveforms is shown in Figure 5 where it can be seen that the high sampling rate allows the visualisation of the waveform in the low energy channel.

3.2. Merger and TapeServer

The data from each of the FEEs connected to the central server is read out and merged by a dedicated Merger program [32]. he program forms TCP (Transmission Control Protocol) links with each of the FEEs to efficiently

read data from their memory buffers as 64 kB blocks. The data from the buffers are then merged into a single time ordered list using the SYNC information items that are embedded in each of the data streams. A second program known as the TapeServer [32] forms an additional TCP link with the output of the merger program. It is the TapeServer that is responsible for writing the data to disk on the AIDA server. Data file names are automatically incremented when the size of the file reaches a pre-determined size (usually configured as 2 GB).

In many cases it is desirable to also forward the data onto other systems while also writing the data to file. Examples of this include running an online data analysis program to monitor the quality of the incoming data and also in forwarding data to other experimental systems to monitor synchronisation between systems. This is achieved by placing a "data spy" on the link between the Merger and the TapeServer, allowing the extraction of data blocks from a shared memory segment in the TapeServer. For example, in recent experiments at GSI this methodology has been used to forward AIDA data onto the MBS DAQ system used by the DESPEC collaboration [33].

3.3. Data sorting and event building

The data recorded by the DAQ consists of a time ordered data stream of of individually timestamped ADC and discriminator data. The actual building of "decay" and "implant" events from this stream requires further analysis which can be done either online during the experiment for a quick analysis or offline for a more complete analysis. The methods used can be split up into four main stages; data unpacking, event building, calibration and clustering.

3.3.1. Unpacking

During the unpacking stage data is read into the program in 64 kB data blocks, from which the data words representing individual data items are extracted. Depending on whether the data item is an ADC item or an information item values for FEE#, Channel, Timestamp and ADC data, or FEE#, information type, information value and Timestamp are obtained respectively. As the timestamp included in each event only contains the least significant bit (LSB) the full timestamp is reconstructed by combining with the most recently updated value of the most significant bit (MSB), which is sent as an information data item. During the unpacker stage the extracted ADC data items are placed into a time ordered list which is then passed onto the event builder stage of the program.

3.3.2. Event building

As each channel in AIDA is self triggered, there is not a conventional "trigger" and "event window" which defines a period in which all ADC events are assumed to be correlated. Instead the correlation of data items must be done during the sorting. The logic with which this is done

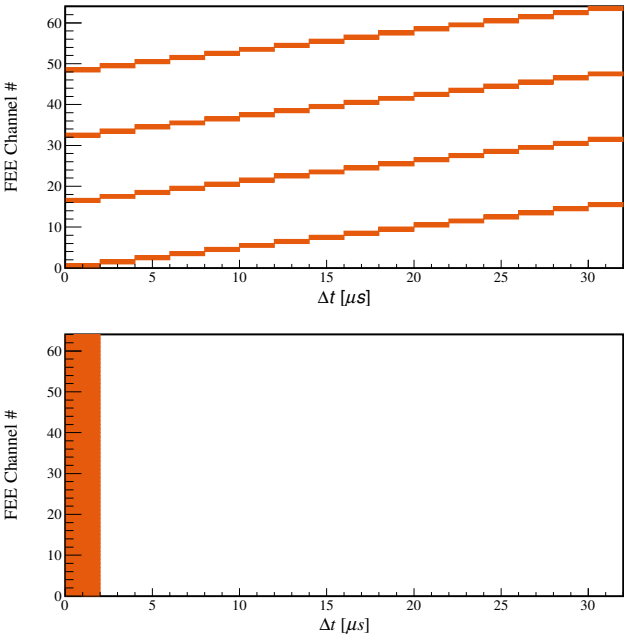

Figure 6: Time distribution of pulser events within a FEE card, relative to the first timestamp recorded for that event. Top plot shows the uncorrected distribution, clearly demonstrating the effect the multiplexer has. The bottom plot shows the distribution once corrected, with the majority of events now observed to occur at the same time.

is dictated by the multiplexed output used in the ASICs and specifically the time period between successive readouts. For example, as the time period between successive readouts in the ASIC is 2 μs, if two adjacent channels in the ASIC simultaneously record an event the first read out will be given a timestamp $t = t_0$ while the second is given a timestamp of $t = t_0 + 2$ μs. As a result we say that there is a chance that all events with a time difference Δt of $\Delta t \leq 2$ μs may be correlated and define gaps between successive events of greater than 2 μs as an event boundary.

With the event boundaries defined it is then necessary to correct the timestamps of items within the window for the delay in read out resulting from the multiplexer. The need for this correction can be clearly seen for events where a pulser signal is input to all FEE64 channels simultaneously, as shown in Figure 6. The upper panel shows the non-timestamp corrected read out time of data items within a FEE with respect to the first timestamp of that event window. The timestamps of successive ASIC channels are observed to increment in 2 μs steps with the first channel of each ASIC being aligned. The timestamps for the multiplexed output are easily corrected by keeping track of the number of data items already recorded by an ASIC within the event window. The result of this correction applied to the pulser events is shown in the lower panel of Figure 6, where it is observed that following the correction that all of the pulser items are now observed to occur at the same time.

After the timestamp correction, the data items within an event window are put into one of two lists depending on whether the data item corresponds to LEC or HEC data. If the event window contains two or more data items that originate from the high energy channel (the minimum number of data items required to determine a position on a DSSD), the event window is defined as an 'implant event' and only the high energy data items are passed on for calibration. The reason only the high energy data items are passed on is due to the large amount of charge deposited in the detector, strips adjacent to the implant location will also observe an amount of charge which could be mistaken as a decay if not rejected. If there are no high-energy data items but the number of low-energy data items is greater than half the total number of strips in the system the event is defined as a 'pulser event' and these data items are filtered out. Finally, if neither of these conditions are fulfilled and there are two or more low-energy data items, the event is defined as a 'decay event' and the low energy data items are passed on for calibration.

3.3.3. Calibration

In the calibration stage the data items are converted from FEE# and channel to DSSD, front (p+n junction) or back (n+n Ohmic) side, and strip. Due to complexities in the DSSD readout and the adaptor board layout there is not a 1:1 mapping between channel number and strip number which must be corrected for during this stage.

For many experiments involving AIDA an absolute energy calibration is not required and a nominal conversion from ADC channel to energy is performed. The first step in this process for the low-energy data items is the correction for the ADC offset. This value is found by performing a pulser walkthrough before/after an experiment, in which pulser signals of known relative amplitudes are fed into the channel. By determining the centroids of the peaks for each channel an ADC offset for each channel can be obtained. A nominal gain of 0.7 keV per ADC channel is then applied to the offset corrected value which is determined by the nominal overall gain of the preamplifier, shaping amplifier, peak hold, MUX and ADC signal processing chain. The variation from channel to channel is dominated by the preamplifier feedback capacitance (C_f). By careful ASIC design and layout the variation of C_f from channel to channel is kept to within c. 3%. ADC offset correction therefore produces ADC data which are gain matched to a few % level, which is sufficient for many applications (e.g. low energy beta events).

For applications where higher precision gain matching is required a method using in beam data has been developed based on the techniques given in Ref. [34]. Traditional calibration sources are not well suited to the calibration of the system due to the challenges of being able to illuminate all detectors within the stack. Instead, in beam light ions, produced during the fragmentation of heavy ion are used. These ions are well suited to calibration as they are not stopped in the silicon and instead punch through the entire detector stack in a straight line, depositing $\approx 1-3$ MeV in individual pixels of each detector. The method presented in Ref. [34] allows these events to be used to provide a relative gain match for all strips on a detector, but not between detectors as the absolute energy deposited by the light ions is not known. An absolute gain match is then found by performing a background run and identifying α-decay events from the naturally occurring Uranium (4n+2) decay series present in the atmosphere.

Once calibrated, the data items are placed into a list sorted by detector, then side, then by strip such that data items from adjacent strips are adjacent events in the list.

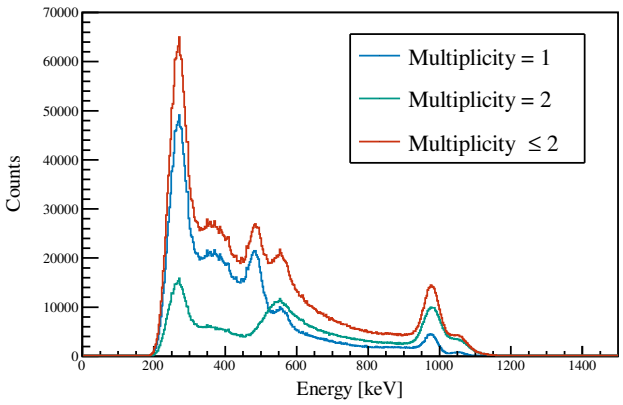

Figure 7: Energy spectrum of a ^{207}Bi conversion electron source gated on different multiplicities of strips firing.

3.3.4. Clustering and pairing

β-electrons can have a range in silicon of greater than the strip pitch of the detector, for example, a 1 MeV electron has a range of 2.3 mm in Si. β-particles may therefore deposit energy across multiple adjacent strips. To account for this the contributions of adjacent strips that produce data within the same event window are summed together to form clusters. The impact of clustering can be seen in Figure 7 which shows the energy spectrum observed for a ^{207}Bi conversion electron source gated on different cluster size multiplicities. When gated on cluster sizes of a single strip (blue line), it can be seen that the majority of electrons observed are low in energy. Some higher energy electrons are observed as it is possible that they propagate through the Si parallel to the direction of the strip. When looking at the energies recorded by clusters of two adjacent strips (green line) the majority of electrons are observed at higher energies, with less observed at lower energies.

The absolute positions of events on the DSSD surface are found by matching clusters from the front side of the detector with the back side of the detector. As both the front and back clusters should record the same energy an equal energy cut is used as a matching condition, reducing the number of random correlations that could otherwise occur. The position of the event is defined to be at the geometric centre of the now 2-dimensional cluster. The

size of the cluster, e.g. the width and height, is also stored which allows the event area to be used in later stages of analysis.

For 'decay' events clustering is performed for all of the detectors present in an event window with the final paired clusters written to an output file in time order. For implant events it is often only the layer in which the ion stops that is required in the final analysis. As such this stopping layer is calculated and only high-energy events occurring in this layer for a given event window are written to file. The stopping layer is defined as the layer in which the following conditions are met: that for both the front and back side of the detector there is at least one high-energy data item in each, that there are no high-energy data items in downstream detectors, that all upstream detectors have at least one high-energy data item in. With these conditions a stopping layer and position can be assigned to the majority of high energy event-windows.

3.4. Implant decay correlations

Correlations between implanted ions and their subsequent decay products are done based on the positional information available for the events. For decay products such as protons and α particles, which have a relatively small range in Si, it is often enough to just look for correlations in the same pixel in which the ion is implanted. However, for β-decays which have a much greater range in Si it is necessary to look for correlations across a wider area. Conventional methods of correlating β-decays with implants in pixelated detectors define an area of a few mm^2 around the implant location and correlate with all decay events that fall within this area. While this method provides a reasonable correlation efficiency it comes at the cost of an increased random contribution. This increased random rate can be down to the narrower strip pitch of the AIDA detectors compared to previous implantation detectors, requiring a greater number of strips to be included in the correlation window. To reduce the random correlation rate a new method was developed that makes use of the full positional information for the events obtained with AIDA and does not just use the central location for implant and decay events. Here correlations are defined between implants and decays when their respective cluster areas on the DSSD surface are either overlapping or adjacent to one another. With this method it was found that the same β-decay detection efficiency could be obtained as with conventional methods, but with a significantly reduced random contribution rate. Detailed discussions of the analysis of implant-decay correlations is provided elsewhere [18, 35]. For detailed discussion of data fitting and the evaluation of random and systematic errors see [36].

4. Summary and Outlook

In this paper the base characteristics of the AIDA detector system have been presented. AIDA has now resulted in two PhDs [36, 37] in which further information can be found. The two systems have been used in successful experimental campaigns at RIBF RIKEN [38, 39, 40, 41] and also at GSI as part of FAIR Phase 0 [42, 43, 44]. Across these campaigns the performance of the systems have been demonstrated with the use of ion gated implant-decay correlations resulting in the measurements of new P_{xn} values and excited state lifetimes. At other laboratories similar systems are currently in development [45]. In the near future it is envisioned that AIDA will continue to be used as the core component of DESPEC with the other setup ready to be run in parallel at RIKEN. During this time the operation of the system will continue to be refined. With the eventual start of "Day 1" science at FAIR, AIDA will be well placed to perform cutting edge science exploiting the radioactive ion beams available via the Super-FRS.

References

[1] J. J. Cowan, C. Sneden, J. E. Lawler, A. Aprahamian, M. Wiescher, K. Langanke, G. Martínez-Pinedo, F.-K. Thielemann, Making the Heaviest Elements in the Universe: A Review of the Rapid Neutron Capture Process, Rev. Mod. Phys. Accepted (jan 2020). arXiv:1901.01410.
URL http://arxiv.org/abs/1901.01410

[2] T. Kubo, In-flight RI beam separator BigRIPS at RIKEN and elsewhere in Japan, Nuclear Instruments and Methods in Physics Research, Section B: Beam Interactions with Materials and Atoms 204 (2003) 97–113. doi:10.1016/S0168-583X(02)01896-7.

[3] S. Hofmann, W. Reisdorf, G. Münzenberg, F. P. Heßberger, J. R. H. Schneider, P. Armbruster, Proton radioactivity of151Lu, Zeitschrift für Physik A Atoms and Nuclei 305 (2) (1982) 111–123. doi:10.1007/BF01415018.
URL http://link.springer.com/10.1007/BF01415018

[4] P. Woods, S. Bennett, M. Freer, B. Fulton, R. Page, K. Connell, R. Cunningham, J. Groves, J. Simpson, A. James, M. Hotchkis, W. Rae, A detection system for the study of alpha and proton radioactivity on the Daresbury recoil mass separator, Nuclear Instruments and Methods in Physics Research Section A: Accelerators, Spectrometers, Detectors and Associated Equipment 276 (1-2) (1989) 195–201. doi:10.1016/0168-9002(89)90632-3.
URL https://linkinghub.elsevier.com/retrieve/pii/0168900289906323

[5] P. J. Sellin, P. J. Woods, R. D. Page, S. J. Bennett, R. A. Cunningham, M. Freer, B. R. Fulton, M. A. C. Hotchkis, A. N. James, The limit of stability of proton-rich thallium isotopes: a search for the decay of177Tl, Zeitschrift für Physik A: Hadrons and Nuclei 338 (2) (1991) 245–246. doi:10.1007/BF01284803.
URL http://link.springer.com/10.1007/BF01284803

[6] P. Sellin, P. Woods, D. Branford, T. Davinson, N. Davis, D. Ireland, K. Livingston, R. Page, A. Shotter, S. Hofmann, R. Hunt, A. James, M. Hotchkis, M. Freer, S. Thomas, A double-sided silicon strip detector system for proton radioactivity studies, Nuclear Instruments and Methods in Physics Research Section A: Accelerators, Spectrometers, Detectors and Associated Equipment 311 (1-2) (1992) 217–223. doi:10.1016/0168-9002(92)90867-4.
URL https://linkinghub.elsevier.com/retrieve/pii/0168900292908674

[7] J. Prisciandaro, A. Morton, P. Mantica, Beta counting system for fast fragmentation beams, Nuclear Instruments and Methods in Physics Research Section A: Accelerators, Spectrometers, Detectors and Associated Equipment 505 (1-2) (2003) 140–143. doi:10.1016/S0168-9002(03)01037-4.

URL https://linkinghub.elsevier.com/retrieve/pii/S0168900203010374

[8] C. B. Hinke, M. Böhmer, P. Boutachkov, T. Faestermann, H. Geissel, J. Gerl, R. Gernhäuser, M. Górska, A. Gottardo, H. Grawe, J. L. Grębosz, R. Krücken, N. Kurz, Z. Liu, L. Maier, F. Nowacki, S. Pietri, Z. Podolyák, K. Sieja, K. Steiger, K. Straub, H. Weick, H. J. Wollersheim, P. J. Woods, N. Al-Dahan, N. Alkhomashi, A. Ataç, A. Blazhev, N. F. Braun, I. T. Čeliković, T. Davinson, I. Dillmann, C. Domingo-Pardo, P. C. Doornenbal, G. De France, G. F. Farrelly, F. Farinon, N. Goel, T. C. Habermann, R. Hoischen, R. Janik, M. Karny, A. Kaşkaş, I. M. Kojouharov, T. Kröll, Y. Litvinov, S. Myalski, F. Nebel, S. Nishimura, C. Nociforo, J. Nyberg, A. R. Parikh, A. Procházka, P. H. Regan, C. Rigollet, H. Schaffner, C. Scheidenberger, S. Schwertel, P. A. Söderström, S. J. Steer, A. Stolz, P. Strmeň, Superallowed Gamow-Teller decay of the doubly magic nucleus 100Sn, Nature 486 (7403) (2012) 341–345. doi:10.1038/nature11116.

[9] S. Nishimura, Beta-gamma spectroscopy at RIBF, Progress of Theoretical and Experimental Physics 2012 (1) (2012) 1–13. doi:10.1093/ptep/pts078.
URL https://academic.oup.com/ptep/article-lookup/doi/10.1093/ptep/pts078

[10] P. J. Woods, Decay spectroscopy of exotic nuclei at fair, Grant number EP/E001734/1, EPSRC (2006).

[11] H. Sakurai, RI Beam Factory Project at RIKEN, Nuclear Physics A 805 (1-4) (2008) 526c–532c. doi:10.1016/j.nuclphysa.2008.02.291.
URL http://dx.doi.org/10.1016/j.nuclphysa.2008.02.291https://linkinghub.elsevier.com/retrieve/pii/S0375947408003862

[12] A. Mistry, H. Albers, T. Arıcı, A. Banerjee, G. Benzoni, B. Cederwall, J. Gerl, M. Górska, O. Hall, N. Hubbard, I. Kojouharov, J. Jolie, T. Martinez, Z. Podolyák, P. Regan, J. Tain, A. Tarifeno-Saldivia, H. Schaffner, V. Werner, G. Ağgez, J. Agramunt, U. Ahmed, O. Aktas, V. Alcayne, A. Algora, S. Alhomaidhi, F. Amjad, C. Appleton, M. Armstrong, M. Balogh, K. Banerjee, P. Bednarczyk, J. Benito, C. Bhattacharya, P. Black, A. Blazhev, S. Bottoni, P. Boutachkov, A. Bracco, A. Bruce, M. Brunet, C. Bruno, I. Burrows, F. Calvino, R. Canavan, D. Cano-Ott, M. Chishti, P. Coleman-Smith, M. Cortés, G. Cortes, F. Crespi, B. Das, T. Davinson, A. De Blas, T. Dickel, M. Doncel, A. Ertoprak, A. Esmaylzadeh, B. Fornal, L. Fraile, F. Galtarossa, A. Gottardo, V. Guadilla, J. Ha, E. Haettner, G. Häfner, H. Heggen, P. Herrmann, C. Hornung, S. Jazrawi, P. John, A. Jokinen, C. Jones, D. Kahl, V. Karayonchev, E. Kazantseva, R. Kern, L. Knafla, R. Knöbel, P. Koseoglou, G. Kosir, D. Kostyleva, N. Kurz, N. Kuzminchuk, M. Labiche, J. Lawson, I. Lazarus, S. Lenzi, S. Leoni, M. Llanos-Expósito, R. Lozeva, A. Maj, J. Meena, E. Mendoza, R. Menegazzo, D. Mengoni, T. Mertzimekis, M. Mikolajczuk, B. Million, N. Mont-Geli, A. Morales, P. Morral, I. Mukha, J. Murias, E. Nacher, P. Napiralla, D. Napoli, B. Nara-Singh, D. O'Donnell, S. Orrigo, R. Page, R. Palit, M. Pallas, J. Pellumaj, S. Pelonis, H. Pentilla, A. Pérez de Rada, R. Pérez-Vidal, C. Petrache, N. Pietralla, S. Pietri, S. Pigliapoco, J. Plaza, M. Polettini, C. Porzio, V. Pucknell, F. Recchia, P. Reiter, K. Rezynkina, S. Rinta-Antila, E. Rocco, H. Rösch, P. Roy, B. Rubio, M. Rudigier, P. Ruotsalainen, S. Saha, E. Şahin, C. Scheidenberger, D. Seddon, L. Sexton, A. Sharma, M. Si, J. Simpson, A. Smith, R. Smith, P. Söderström, A. Sood, A. Soylu, Y. Tanaka, J. Valiente-Dobón, P. Vasileiou, J. Vasiljevic, J. Vesic, D. Villamarin, H. Weick, M. Wiebusch, J. Wiederhold, O. Wieland, H. Wollersheim, P. Woods, A. Yaneva, I. Zanon, G. Zhang, J. Zhao, R. Zidarova, G. Zimba, A. Zyriliou, The DESPEC setup for GSI and FAIR, Nuclear Instruments and Methods in Physics Research Section A: Accelerators, Spectrometers, Detectors and Associated Equipment 1033 (April) (2022) 166662. doi:10.1016/j.nima.2022.166662.
URL https://linkinghub.elsevier.com/retrieve/pii/S0168900222002170

[13] A. Tarifeño-Saldivia, J. Tain, C. Domingo-Pardo, F. Calviño, G. Cortés, V. Phong, A. Riego, J. Agramunt, A. Algora, N. Brewer, R. Caballero-Folch, P. Coleman-Smith, T. Davinson, I. Dillmann, A. Estradé, C. Griffin, R. Grzywacz, L. Harkness-Brennan, G. Kiss, M. Kogimtzis, M. Labiche, I. Lazarus, G. Lorusso, K. Matsui, K. Miernik, F. Montes, A. Morales, S. Nishimura, R. Page, Z. Podolyák, V. Pucknell, B. Rasco, P. Regan, B. Rubio, K. Rykaczewski, Y. Saito, H. Sakurai, J. Simpson, E. Sokol, R. Surman, A. Svirkhin, S. Thomas, A. Tolosa, P. Woods, Conceptual design of a hybrid neutron-gamma detector for study of β-delayed neutrons at the RIB facility of RIKEN, Journal of Instrumentation 12 (04) (2017) P04006–P04006. arXiv:1606.05544, doi:10.1088/1748-0221/12/04/P04006.
URL http://stacks.iop.org/1748-0221/12/i=04/a=P04006?key=crossref.d973a25dbe6ced99e01c541d18ddeaeehttp://arxiv.org/abs/1606.05544http://dx.doi.org/10.1088/1748-0221/12/04/P04006https://iopscience.iop.org/article/10.1088/1748-0221/12/04/P04006

[14] J. Tain, A. Algora, J. Agramunt, V. Guadilla, M. Jordan, A. Montaner-Pizá, B. Rubio, E. Valencia, D. Cano-Ott, W. Gelletly, T. Martinez, E. Mendoza, Z. Podolyák, P. Regan, J. Simpson, A. Smith, J. Strachan, A decay total absorption spectrometer for DESPEC at FAIR, Nuclear Instruments and Methods in Physics Research Section A: Accelerators, Spectrometers, Detectors and Associated Equipment 803 (2015) 36–46. doi:10.1016/j.nima.2015.09.009.
URL http://dx.doi.org/10.1016/j.nima.2015.09.009https://linkinghub.elsevier.com/retrieve/pii/S016890021501058X

[15] M. Rudigier, Z. Podolyák, P. H. Regan, A. M. Bruce, S. Lalkovski, R. L. Canavan, E. R. Gamba, O. Roberts, I. Burrows, D. M. Cullen, L. M. Fraile, L. Gerhard, J. Gerl, M. Gorska, A. Grant, J. Jolie, V. Karayonchev, N. Kurz, W. Korten, I. H. Lazarus, C. R. Nita, V. F. Pucknell, J. M. Régis, H. Schaffner, J. Simpson, P. Singh, C. M. Townsley, J. F. Smith, J. Vesic, FATIMA — FAst TIMing Array for DESPEC at FAIR, Nuclear Instruments and Methods in Physics Research, Section A: Accelerators, Spectrometers, Detectors and Associated Equipment 969 (January) (2020) 163967. doi:10.1016/j.nima.2020.163967.
URL https://doi.org/10.1016/j.nima.2020.163967

[16] G. S. Li, R. Lozeva, I. Kojouharov, J. Gerl, M. Górska, Characteristics of the DEGAS-FATIMA Hybrid setup for the DESPEC program at NUSTAR, Nuclear Instruments and Methods in Physics Research, Section A: Accelerators, Spectrometers, Detectors and Associated Equipment 987 (October 2020) (2021). doi:10.1016/j.nima.2020.164806.

[17] M. Doncel, B. Cederwall, A. Gadea, J. Gerl, I. Kojouharov, S. Martin, R. Palit, B. Quintana, Nuclear Instruments and Methods in Physics Research A Performance and imaging capabilities of the DEGAS high-resolution γ -ray detector array for the DESPEC experiment at FAIR, Nuclear Inst. and Methods in Physics Research, A 873 (2017) 36–38. doi:10.1016/j.nima.2017.04.019.
URL http://dx.doi.org/10.1016/j.nima.2017.04.019

[18] A. Tolosa-Delgado, J. Agramunt, J. Tain, A. Algora, C. Domingo-Pardo, A. Morales, B. Rubio, A. Tarifeño-Saldivia, F. Calviño, G. Cortes, N. Brewer, B. Rasco, K. Rykaczewski, D. Stracener, J. Allmond, R. Grzywacz, R. Yokoyama, M. Singh, T. King, M. Madurga, S. Nishimura, V. Phong, S. Go, J. Liu, K. Matsui, H. Sakurai, G. Kiss, T. Isobe, H. Baba, S. Kubono, N. Fukuda, D. Ahn, Y. Shimizu, T. Sumikama, H. Suzuki, H. Takeda, P. Söderström, M. Takechi, C. Bruno, T. Davinson, C. Griffin, O. Hall, D. Kahl, P. Woods, P. Coleman-Smith, M. Labiche, I. Lazarus, P. Morrall, V. E. Pucknell, J. Simpson, S. Thomas, M. Prydderch, L. Harkness-Brennan, R. Page, I. Dillmann, R. Caballero-Folch, Y. Saito, A. Estrade, N. Nepal, F. Montes, G. Lorusso, J. Liang, S. Bae, J. Ha, B. Moon, Commissioning of the BRIKEN detector

for the measurement of very exotic ¡math altimg="si79.gif" display="inline" id="d1e946" overflow="scroll"¿ ¡mi¿β¡/mi¿ ¡/math¿ -delayed neutron emitters, Nuclear Instruments and Methods in Physics Research Section A: Accelerators, Spectrometers, Detectors and Associated Equipment 925 (2019) 133–147. arXiv:1808.00732, doi:10.1016/j.nima.2019.02.004.
URL http://arxiv.org/abs/1808.00732https://linkinghub.elsevier.com/retrieve/pii/S0168900219301743

[19] H. Geissel, H. Weick, M. Winkler, G. Münzenberg, V. Chichkine, M. Yavor, T. Aumann, K. Behr, M. Böhmer, A. Brünle, K. Burkard, J. Benlliure, D. Cortina-Gil, L. Chulkov, A. Dael, J.-E. Ducret, H. Emling, B. Franczak, J. Friese, B. Gastineau, J. Gerl, R. Gernhäuser, M. Hellström, B. Jonson, J. Kojouharova, R. Kulessa, B. Kindler, N. Kurz, B. Lommel, W. Mittig, G. Moritz, C. Mühle, J. Nolen, G. Nyman, P. Roussell-Chomaz, C. Scheidenberger, K.-H. Schmidt, G. Schrieder, B. Sherrill, H. Simon, K. Sümmerer, N. Tahir, V. Vysotsky, H. Wollnik, A. Zeller, The Super-FRS project at GSI, Nuclear Instruments and Methods in Physics Research Section B: Beam Interactions with Materials and Atoms 204 (2003) 71–85. doi:10.1016/S0168-583X(02)01893-1.
URL https://linkinghub.elsevier.com/retrieve/pii/S0168583X02018931

[20] R. Krücken, The NuSTAR facilty at FAIR, Journal of Physics G: Nuclear and Particle Physics 31 (10) (2005). doi:10.1088/0954-3899/31/10/077.

[21] K.-H. Schmidt, J. Benlliure, A. Junghans, Fission of nuclei far from stability, Nuclear Physics A 693 (1-2) (2001) 169–189. doi:10.1016/S0375-9474(01)00648-0.
URL https://linkinghub.elsevier.com/retrieve/pii/S0375947401006480

[22] Samtec, Samtexc ftsh header (2022).
URL https://www.samtec.com/products/ftsh

[23] Samtec, Samtexc ffsd ribbon cable (2022).
URL https://www.samtec.com/products/ffsd

[24] ERNI, Erni ermet (2022).
URL https://www.erni.com/en/products-and-solutions/electronic-connectors/ermet-connectors

[25] M. S. Ltd., Micron semiconductor ltd. (2022).
URL http://www.micronsemiconductor.co.uk/

[26] D. Braga, P. Coleman-Smith, T. Davinson, I. Lazarus, R. Page, S. Thomas, AIDA: A 16-channel amplifier ASIC to read out the advanced implantation detector array for experiments in nuclear decay spectroscopy, in: 2009 IEEE Nuclear Science Symposium Conference Record (NSS/MIC), IEEE, 2009, pp. 1924–1928. doi:10.1109/NSSMIC.2009.5402153.
URL http://ieeexplore.ieee.org/document/5402153/

[27] A. Devices, Ad7980 (2022).
URL https://www.analog.com/en/products/ad7980.html

[28] Xilinx, Xilinx virtex 5 (2022).
URL https://www.xilinx.com/

[29] I. Lazarus, E. Appelbe, P. Butler, P. Coleman-Smith, J. Cresswell, S. Freeman, R. Herzberg, I. Hibbert, D. Joss, S. Letts, R. Page, V. Pucknell, P. Regan, J. Sampson, J. Simpson, J. Thornhill, R. Wadsworth, The GREAT triggerless total data readout method, IEEE Transactions on Nuclear Science 48 (3) (2001) 567–569. doi:10.1109/23.940120.
URL http://ieeexplore.ieee.org/document/940120/

[30] A. Devices, Ad9252 (2022).
URL https://www.analog.com/en/products/ad9252.html

[31] P. Jansweijer, H. Peek, E. de Wolf, White Rabbit: Sub-nanosecond timing over Ethernet, Nuclear Instruments and Methods in Physics Research Section A: Accelerators, Spectrometers, Detectors and Associated Equipment 725 (2013) 187–190. doi:10.1016/j.nima.2012.12.096.
URL https://linkinghub.elsevier.com/retrieve/pii/S016890021201652X

[32] S. D. Laboratory, Midas (2022).
URL http://npg.dl.ac.uk/MIDAS/

[33] H. Essel, N. Kurz, The general purpose data acquisition system MBS, in: 1999 IEEE Conference on Real-Time Computer Applications in Nuclear Particle and Plasma Physics. 11th IEEE NPSS Real Time Conference. Conference Record (Cat. No.99EX295), IEEE, 1999, pp. 475–478. doi:10.1109/RTCON.1999.842672.
URL http://ieeexplore.ieee.org/document/842672/

[34] M. Reese, J. Gerl, P. Golubev, N. Pietralla, Nuclear Instruments and Methods in Physics Research A Automatic intrinsic calibration of double-sided silicon strip detectors, Nuclear Inst. and Methods in Physics Research, A 779 (2015) 63–68. doi:10.1016/j.nima.2015.01.032.
URL http://dx.doi.org/10.1016/j.nima.2015.01.032

[35] B. C. Rasco, N. T. Brewer, R. Yokoyama, R. Grzywacz, K. P. Rykaczewski, A. Tolosa-Delgado, J. Agramunt, J. L. Taín, A. Algora, O. Hall, C. Griffin, T. Davinson, V. H. Phong, J. Liu, S. Nishimura, G. G. Kiss, N. Nepal, A. Estrade, The ORNL analysis technique for extracting β-delayed multi-neutron branching ratios with BRIKEN, Nuclear Instruments and Methods in Physics Research, Section A: Accelerators, Spectrometers, Detectors and Associated Equipment 911 (September) (2018) 79–86. doi:10.1016/j.nima.2018.09.121.
URL https://doi.org/10.1016/j.nima.2018.09.121

[36] O. Hall, β-delayed neutron emission from r-process nuclei along the $N = 82$ shell closure, Thesis, University of Edinburgh, University of Edinburgh, EH9 3FD, https://era.ed.ac.uk/handle/1842/37296 (July 2020).

[37] C. J. Griffin, β-decay studies of r-process nuclei using the Advanced Implantation Detector Array (AIDA), Thesis, University of Edinburgh, University of Edinburgh, EH9 3FD, https://era.ed.ac.uk/handle/1842/35679 (July 2019).

[38] O. Hall, T. Davinson, A. Estrade, J. Liu, G. Lorusso, F. Montes, S. Nishimura, V. Phong, P. Woods, J. Agramunt, D. Ahn, A. Algora, J. Allmond, H. Baba, S. Bae, N. Brewer, C. Bruno, R. Caballero-Folch, F. Calviño, P. Coleman-Smith, G. Cortes, I. Dillmann, C. Domingo-Pardo, A. Fijalkowska, N. Fukuda, S. Go, C. Griffin, R. Grzywacz, J. Ha, L. Harkness-Brennan, T. Isobe, D. Kahl, L. Khiem, G. Kiss, A. Korgul, S. Kubono, M. Labiche, I. Lazarus, J. Liang, Z. Liu, K. Matsui, K. Miernik, B. Moon, A. Morales, P. Morrall, M. Mumpower, N. Nepal, R. Page, M. Piersa, V. Pucknell, B. Rasco, B. Rubio, K. Rykaczewski, H. Sakurai, Y. Shimizu, D. Stracener, T. Sumikama, H. Suzuki, J. Tain, H. Takeda, A. Tarifeño-Saldivia, A. Tolosa-Delgado, M. Wolińska-Cichocka, R. Yokoyama, β-delayed neutron emission of r-process nuclei at the N = 82 shell closure, Physics Letters B 816 (2021) 136266. doi:10.1016/j.physletb.2021.136266.
URL https://linkinghub.elsevier.com/retrieve/pii/S0370269321002069

[39] R. Yokoyama, R. Grzywacz, B. C. Rasco, N. Brewer, K. P. Rykaczewski, I. Dillmann, J. L. Tain, S. Nishimura, D. S. Ahn, A. Algora, J. M. Allmond, J. Agramunt, H. Baba, S. Bae, C. G. Bruno, R. Caballero-Folch, F. Calvino, P. J. Coleman-Smith, G. Cortes, T. Davinson, C. Domingo-Pardo, A. Estrade, N. Fukuda, S. Go, C. J. Griffin, J. Ha, O. Hall, L. J. Harkness-Brennan, J. Heideman, T. Isobe, D. Kahl, M. Karny, T. Kawano, L. H. Khiem, T. T. King, G. G. Kiss, A. Korgul, S. Kubono, M. Labiche, I. Lazarus, J. Liang, J. Liu, G. Lorusso, M. Madurga, K. Matsui, K. Miernik, F. Montes, A. I. Morales, P. Morrall, N. Nepal, R. D. Page, V. H. Phong, M. Piersa, M. Prydderch, V. F. Pucknell, M. M. Rajabali, B. Rubio, Y. Saito, H. Sakurai, Y. Shimizu, J. Simpson, M. Singh, D. W. Stracener, T. Sumikama, R. Surman, H. Suzuki, H. Takeda, A. Tarifeño-Saldivia, S. L. Thomas, A. Tolosa-Delgado, M. Wolińska-Cichocka, P. J. Woods, X. X. Xu, Strong one-neutron emission from two-neutron unbound states in β decays of the r -process nuclei Ga 86,87, Physical Review C 100 (3) (2019) 1–6. doi:10.1103/PhysRevC.100.031302.

[40] G. G. Kiss, A. Vitéz-Sveiczer, Y. Saito, A. Tarifeño-Saldivia, M. Pallas, J. L. Tain, I. Dillmann, J. Agramunt, A. Algora, C. Domingo-Pardo, A. Estrade, C. Appleton, J. M.

Allmond, P. Aguilera, H. Baba, N. T. Brewer, C. Bruno, R. Caballero-Folch, F. Calvino, P. J. Coleman-Smith, G. Cortes, T. Davinson, N. Fukuda, Z. Ge, S. Go, C. J. Griffin, R. K. Grzywacz, O. Hall, A. Horváth, J. Ha, L. J. Harkness-Brennan, T. Isobe, D. Kahl, T. T. King, A. Korgul, S. Kovács, R. Krücken, S. Kubono, M. Labiche, J. Liu, J. Liang, M. Madurga, K. Miernik, F. Molina, A. I. Morales, M. R. Mumpower, E. Nacher, A. Navarro, N. Nepal, S. Nishimura, M. Piersa-Siłkowska, V. Phong, B. C. Rasco, B. Rubio, K. P. Rykaczewski, J. Romero-Barrientos, H. Sakurai, L. Sexton, Y. Shimizu, M. Singh, T. Sprouse, T. Sumikama, R. Surman, H. Suzuki, T. N. Szegedi, H. Takeda, A. Tolosa, K. Wang, M. Wolinska-Cichocka, P. Woods, R. Yokoyama, Z. Xu, Measuring the β-decay Properties of Neutron-rich Exotic Pm, Sm, Eu, and Gd Isotopes to Constrain the Nucleosynthesis Yields in the Rare-earth Region, The Astrophysical Journal 936 (2) (2022) 107. doi:10.3847/1538-4357/ac80fc.
URL https://iopscience.iop.org/article/10.3847/1538-4357/ac80fc

[41] V. H. Phong, et al., β-delayed one and two neutron emission probabilities south-east of ^{132}Sn and the odd-even systematics in r-process nuclide abundances accepted, Physical Review Letters (Sep 2022).
URL https://journals.aps.org/prl/accepted/1a073YefG481267fd88f94946ccaedb3769653746

[42] S. Jazrawi, A. Yaneva, M. Polettini, B. Das, P. Regan, M. Górska, B. Cederwall, J. Jolie, H. Albers, M. Chishti, A. Banerjee, N. Hubbard, A. Mistry, M. Rudigier, G. Benzoni, J. Gerl, A. Bruce, Z. Podolyák, B. Nara Singh, G. Zhang, S. Alhomaidhi, C. Appleton, T. Arici, A. Blazhev, T. Davinson, A. Esmaylzadeh, L. Fraile, G. Häfner, O. Hall, P. John, V. Karayonchev, I. Koujoharov, N. Kurz, M. Mikolajczuk, N. Pietralla, S. Pietri, J. Regis, E. Sahin, L. Sexton, H. Schaffner, C. Scheidenberger, A. Sharma, J. Vesic, H. Weick, V. Werner, R. Lozeva, M. Si, Commissioning the FAst TIMing array (FATIMA) at FAIR Phase-0: Half-lives of excited states in the N=50 isotones 96Pd and 94Ru, Radiation Physics and Chemistry (May) (2022) 110234. doi:10.1016/j.radphyschem.2022.110234.
URL https://linkinghub.elsevier.com/retrieve/pii/S0969806X22002766

[43] B. Das, B. Cederwall, C. Qi, M. Górska, P. H. Regan, Aktas, H. M. Albers, A. Banerjee, M. M. Chishti, J. Gerl, N. Hubbard, S. Jazrawi, J. Jolie, A. K. Mistry, M. Polettini, A. Yaneva, S. Alhomaidhi, J. Zhao, T. Arici, S. Bagchi, G. Benzoni, P. Boutachkov, T. Davinson, T. Dickel, E. Haettner, O. Hall, C. Hornung, J. P. Hucka, P. R. John, I. Kojouharov, R. Knöbel, D. Kostyleva, N. Kuzminchuk, I. Mukha, W. R. Plass, B. S. Nara Singh, J. Vasiljević, S. Pietri, Z. Podolyák, M. Rudigier, H. Rösch, E. Sahin, H. Schaffner, C. Scheidenberger, F. Schirru, A. Sharma, R. Shearman, Y. Tanaka, J. Vesić, H. Weick, H. J. Wollersheim, U. Ahmed, A. Algora, C. Appleton, J. Benito, A. Blazhev, A. Bracco, A. M. Bruce, M. Brunet, R. Canavan, A. Esmaylzadeh, L. M. Fraile, G. Häfner, H. Heggen, D. Kahl, V. Karayonchev, R. Kern, A. Korgul, G. Kosir, N. Kurz, R. Lozeva, M. Mikolajczuk, P. Napiralla, R. Page, C. M. Petrache, N. Pietralla, J. M. Régis, P. Ruotsalainen, L. Sexton, V. Sanchez-Temble, M. Si, J. Vilhena, V. Werner, J. Wiederhold, W. Witt, P. J. Woods, G. Zimba, Nature of seniority symmetry breaking in the semimagic nucleus Ru 94, Physical Review C 105 (3) (2022) 1–6. doi:10.1103/PhysRevC.105.L031304.

[44] M. Polettini, J. Pellumaj, G. Benzoni, J. J. Valiente-Dobón, G. Zhang, D. Mengoni, R. M. Vidal, D. Genna, A. Bracco, G. Aggez, U. Ahmed, Aktas, M. Al Aqueel, B. Alayed, H. M. Albers, A. Algora, S. Alhomaidhi, C. Appleton, T. Arici, M. Armstrong, K. Arnswald, M. Balogh, A. Banerjee, J. B. García, A. Blazhev, S. Bottoni, P. Boutachkov, A. Bruce, C. Bruno, F. Camera, B. Cederwall, M. M. Chishti, M. L. Cortés, D. M. Cox, F. C. Crespi, B. Das, T. Davinson, G. De Angelis, T. Dickel, M. Doncel, R. Donthi, A. Ertoprak, R. Escudeiro, A. Esmaylzadeh, L. M. Fraile, L. Gaffney, E. R. Gamba, J. Gerl, M. Górska, A. Gottardo, J. Ha, E. Haettner, O. Hall, H. Heggen, Y. Hrabar, N. Hubbard, S. Jazrawi, P. R. John, J. Jolie, C. Jones, D. Joss, D. Judson, D. Kahl, V. Karayonchev, E. Kazantseva, R. Kern, L. Knafla, I. Kojouharov, A. Korgul, W. Korten, P. Koseoglou, G. Kosir, D. Kostyleva, T. Kurtukian-Nieto, N. Kurz, N. Kuzminchuk, M. Labiche, S. Lenzi, S. Leoni, M. L. Expósito, R. Lozeva, T. J. Mertzimekis, M. Mikolajczuk, B. Million, A. K. Mistry, A. Morales, I. Mukha, J. R. Murias, D. Napoli, B. S. Singh, D. O'Donnell, S. E. Orrigo, R. Page, S. Pelonis, J. Petrovic, N. Pietralla, S. Pietri, S. Pigliapoco, Z. Podolyak, C. Porzio, B. Q. Arnes, F. Recchia, P. H. Regan, J. M. Régis, P. Reiter, K. Rezynkina, P. Roy, M. Rudigier, P. Ruotsalainen, E. Sahin, L. G. Sarmiento, M. M. Satrazani, H. Schaffner, C. Scheidenberger, L. Sexton, A. Sharma, J. Smallcombe, P. A. Söderström, A. Sood, P. Vasileiou, J. Vesic, J. Vilhena, L. Waring, H. Weick, V. Werner, J. Wiederhold, O. Wieland, K. Wimmer, H. J. Wollersheim, P. Woods, A. Yaneva, I. Zanon, J. Zhao, R. Zidarova, S. Ziliani, G. Zimba, A. Zyriliou, Decay studies in the $A \sim 225$ Po-Fr region from the DESPEC campaign at GSI in 2021, Nuovo Cimento della Societa Italiana di Fisica C 45 (5) (2022) 225–228. doi:10.1393/ncc/i2022-22125-5.

[45] FRIB Decay Sation Working Group, The FRIB Decay Station White Paper, Tech. rep., https://fds.ornl.gov/wp-content/uploads/2020/09/FDS-WP.pdf (01 2019).